Theoretical and Applied Fracture Mechanics 134 (2024) 104711

Contents lists available at ScienceDirect

Theoretical and Applied Fracture Mechanics

journal homepage: www.elsevier.com/locate/tafmec

Effect of length-to-height ratio on fracture properties of asymmetrical single-edge notched beam (ASENB) specimen made of ceramic under full range mixed mode I/II loading state

Tang Qiong [a], Haytham F. Isleem [c,d], Hamid Reza Karimi [b,*]

[a] School of Applied Technologies, Qujing Normal University, Qujing 655011, Yunnan, China
[b] School of Civil Engineering, Iran University of Science and Technology, Tehran, Iran
[c] Jadara University Research Center, Jadara University, Irbid, Jordan.
[d] Department of computer Science, University of York, York YO10 5DD, United Kingdom.

ARTICLE INFO

Keywords:
Single-edge notched beam
Mode I/II fracture
Finite element
Geometry effect
Ceramic

ABSTRACT

Asymmetrical single-edge notched beam (ASENB) specimen is among the suitable specimens for measuring full mode I/II fracture parameters. However, in lack of a standard or common method, researchers used this specimen with different geometers, which have proven can affect the results. This research evaluated the effect of ASENB's geometry on fracture parameters numerically and experimentally. First, the finite element method determined the geometry factors (Y_I and Y_{II}) and non-singular (T-stress) fracture parameters. Then, the experimental fracture tests were conducted using ceramic material. Results show it is more reasonable to express the Y_I and Y_{II} based on S_1/L and S_2/H, instant S_1/L, and S_2/L. In other words, the geometry factors can be expressed better based on the height of the specimen and not length. So, for ASENB specimens tested in conventional S_1/L of 0.7 to 0.9, the pure mode-II condition was generated in $0.05 < S_2/H < 0.14$. The modeling showed that the non-singular term of fracture (T-stress) was significant compared to fracture toughness, so the Biaxiality was measured as 0.5 to -2.5, more significant for pure mode-II and almost regardless of the a/H ratio. As experimental tests show, the relative length of the ASENB specimen has an insignificant effect on measured fracture toughness, so a more compact specimen with L/H of about 2 to 4 can suggested for tests.

1. Introduction

Fracture studies require the implementation of suitable methods and techniques, including the use of specimens. Specimens are representative samples of the under investigation material or structure and play a crucial role in experimental studies [1,2]. These specimens should be carefully designed, prepared to simulate real-life conditions, and subjected to controlled loading or stress. By studying the behavior of these specimens under different loading conditions, researchers can observe and analyze the crack growth and failure mechanisms [3].

Various testing methods are employed to investigate cracking behavior in materials and structures. One common method is standard tensile or bending tests, where the specimen is subjected to specific loads until failure occurs. This allows for the measurement of load–displacement or load-time curves, which provide valuable data on the crack initiation and propagation stages [4,5]. One of the tools in developing experimental methods is numerical modeling. Computational tools like finite element analysis can simulate the response and predict crack formation and propagation in fracture mechanics. These models enable researchers to assess the structural integrity, identify critical areas prone to cracking, and develop preventive measures [6,7].

The rectangular edge cracked beam is a commonly used test specimen for fracture toughness experiments [8–10]. This specimen has been used to study fracture phenomena in brittle engineering materials; and designed to simulate different loading conditions and evaluate the fracture toughness of materials such as ceramics, glass, polymers, adhesives, rocks, graphite, composites, and metals [11,12]. The rectangular edge cracked beam specimen offers several advantages. Its simple geometry allows for easy fabrication and testing. Additionally, it provides a controlled and well-defined crack geometry, which is essential

* Corresponding author.
E-mail addresses: tangqiong@mail.qjnu.edu.cn (T. Qiong), mps565@york.ac.uk, isleemhaytham88@gmail.com (H.F. Isleem), Karimi_H@civileng.iust.ac.ir (H.R. Karimi).

https://doi.org/10.1016/j.tafmec.2024.104711
Received 10 July 2024; Received in revised form 11 September 2024; Accepted 5 October 2024
Available online 9 October 2024
0167-8442/

for accurately measuring crack growth and analyzing fracture behavior. Subjected to symmetrical three or four-point bend loading, historically, this specimen is used to create mode I (opening) fracture condition; however, recently, by using asymmetrical supports (or inclining the crack), combinations of mode II (shearing) fracture were also simulated [13–16].

It is worth noting that while rectangular edge cracked beams are commonly used, other test specimens and methods are also employed to investigate mixed-mode fracture. These can include compact tension specimens, modified chevron-notch specimens, notched round bars, and various other geometries tailored to specific research needs. Each specimen type offers its advantages and limitations, and the choice depends on the material properties, desired mode mixity, and research objectives [17–19].

The use of Single-Edge Notched Beam (SENB) specimens for fracture toughness testing raises several debatable issues, including the size and geometry of the specimen. These factors are essential as they can influence the reliability and validity of the test results. The size of the specimen refers to its overall dimensions, often compared to material-specific indicators such as grain size in rocks or aggregate size in concrete. On this issue, the size of the specimen should be larger than a specific level to make an appropriate size, which is crucial for obtaining reliable data [20–22].

The specimen's geometry refers to the ratios of its dimensions, such as the length-to-height ratio, which affects the longitudinal stress distributions in the specimen during testing. Or the height-to-thickness ratio, which influences the transverse stress distribution. Depending on the testing conditions, the specimen may be subjected to either plain stress or plain strain conditions. The height-to-thickness ratio should be chosen carefully to ensure the stress distribution matches the desired condition. Deviations from the intended stress state can affect the initiation and propagation of cracks, compromising the accuracy of fracture toughness measurements [23–25].

Knowing the selection of specimen size is dependent on the type of material and geometry can have an impact on the test results regardless of the material's inherent characteristics, researchers have proposed some general rules for determining the minimum size of test specimens, taking into account various factors specific to the material under investigation. For example, in the works of different researchers on asphalt and concrete materials, where large-size aggregates are present, they proposed that the minimum size of the specimen (the ligament) should be at least three times larger than the maximum size of the aggregates. This ensures that the specimen's ligament represents the base material [16,19,23].

1.1. Literature review

Up to here, the importance of specimen type, the considered geometry, and it's size was discussed. Although several studies have been conducted in this field of study, there is also a need for further studies, even for well-known specimens such as SENB. Among some studies on this matter, Aliha and Mousavi [26], and Mousavi et al. [27] introduced a new test setup for studying mixed-mode I/II fracture toughness. This configuration allows the simulation of pure mode I, II, and intermediate mode mixities using a beam specimen with a small length ratio (with a length typically about three times the height).

Aliha et al. also suggest a beam-shaped specimen with an inclined crack orientation. They see that the ratio of support span to height should be less than one, if the coverage of all mode I and II mixes is needed. They conclude that this specimen has the practical ability for experimental fracture toughness tests for the mode I and II mixes. However, as a severe issue, introducing a precise inclined crack must be done very carefully [28].

Avoiding the difficulties of preparation of single-edge notched bend beams with inclined cracks, Aliha et al. introduced asymmetrical single-edge notched bend beams for simulating the full range of mixed mode I/II. The fracture parameters, including intensity factors and T-stress, were determined with the help of finite element analysis, considering different crack lengths and support distances. Then, the specimen's ability was examined by conducting several fracture tests on a brittle material. The fracture toughness values, the direction of crack initiation, and the crack trajectory were investigated using theoretical fracture mechanics criteria [29].

In other work on asphalt material, Saed et al. used a short seam bending (SBB) specimen in asymmetric load conditions to investigate mixed-mode I/II fracture behavior. Their results showed a significant similarity between the results of SCB and SBB specimens. In pure mode-I and II, a difference of about 15 % is seen between the results of SBB and SCB specimens [30].

Finally, it should be noted, when comparing the works of Aliha et al. and Saed et al., who respectively conducted tests on PMMA (a polymer) and asphalt mixtures using the same (asymmetrical short bend beam) ASENB specimen, it is observed that PMMA, being a homogeneous material without grains or aggregates, requires much smaller sample sizes compared to asphalt. To compare, Aliha et al. used a smaller ASENB specimen, while Saed et al. utilized a larger ASENB specimen with dimensions suitable for testing asphalt mixtures. So, on this basis, it can be said that size and geometry are also important when determining material's characteristics and behavior besides the type of specimen. Materials with distinct features, such as aggregates or grains, may require larger specimens to adequately represent those features, while homogeneous materials like polymers may allow for smaller specimen sizes [31].

1.2. Aims and scope

As discussed, investigating cracking in structures is a complex and multidisciplinary field that requires a combination of scientific research, experimental testing, and numerical modeling. By understanding the behavior of cracks and their causes, researchers can develop effective strategies to predict, prevent, and mitigate the failure of structures, ultimately ensuring their safety and longevity.

The use of different test specimens, including rectangular edge cracked beams, has contributed to the understanding of mixed mode I/II fracture in various engineering materials. These experiments provide valuable insights into fracture behavior, aiding in developing materials with improved toughness and designing structures with enhanced resistance to crack propagation. This is however the size and geometry of SENB specimens have impact on the results of fracture testing. The specimen size should represent the structure, while the geometry should be chosen to achieve the desired stress state. Careful selection of these parameters is essential for obtaining reliable fracture data, allowing for accurate assessment of material behavior and the design of components.

Seen this issue, in the current study it is tried to investigate the effects of the specimen's configuration on the fracture results. These effects were studied for the full range of mode I/II fracture conditions. the study was separated into two sections, numerical and experimental study. First, in the numerical study, ASENB specimens with different relative lengths ($L/H = 2$, 4, 8, and 15), relative crack lengths ($a/H = 0.2$, 0.4, and 0.6), and a wide range of mode mixities ($0.0 \leq M^e \leq 1.0$) were simulated in a finite element software to extract the fracture parameters. In this regard, the $L/H = 2$ is the minimum size of specimen recommended by Aliha et al [26,28], the L/H in the range 4 to 8 are the recommendation of standards such as ASTM D5045 (for fracture tests of plastics) and ASTM E399 (for fracture tests of metals) for fracture toughness measuring of plastic materials), and $L/H = 15$ is the maximum size for a practical SENB specimen made of conventional materials. Then, in an experimental study, using 48 samples, the practical abilities of ASENB specimens were evaluated. As some important aspects of fracture mechanics studies, in current research, the fracture parameters (geometry factors, T-stresses, crack propagation angles) were extracted and justified, also to increase the innovation of the study, the experimental program was done using porcelain material as a brittle material.

2. Materials and methods

The geometry and loading configuration of the ASENB specimen is illustrated in Fig. 1. ASENB is a beam subjected to three-point bend loading with a length of L, a height of H, and a thickness of t. The pure mode-I (fracture in pure tensile mode) occurs when the specimen is loaded symmetrically. To change the state of tensile and shear stresses, the specimen should be subjected to asymmetric loading by adjusting the supports (i.e., S_1 and S_2).

The distance S_2 altered from a symmetrical ($S_1 = S_2$) by moving the support for any fixed value of S_1. A. The contribution of in-plane shear force (representing mode II deformation) becomes more pronounced than the bending moment effect (representing mode I or opening mode) as the S_2 distance decreases. It is also important to consider that the stress distribution in the crack's tip and the resulting mode-mixing may be influenced by the pre-crack length ratio to the specimen height (a/H).

The state of mode mixity in the ASENB specimen is altered by modifying the geometry and loading parameters, including S_1/L, S_2/L, and a/H. both mode I and mode II of the can contribute to this specimen. The ASENB specimen's mode I and mode II stress intensity factors (SIF or K_{Ic} and K_{IIc}) can be expressed as follows [29]:

$$K_{Ic} = \frac{6P_cS_1S_2}{tW^2(S_1 + S_2)}\sqrt{\pi a}Y_I \tag{1}$$

$$K_{IIc} = \frac{6P_cS_1S_2}{tW^2(S_1 + S_2)}\sqrt{\pi a}Y_{II} \tag{2}$$

where Y_I and Y_{II} are geometry factors for modes I and II, respectively. Geometry factors depend on crack length (a/W), and span ratios (S_1/L and S_2/L).

Where the stress field at crack's tip can be described by the stress intensity factors in relation to the singular stress term, the non-singular stress term in this series expansion is called T-stress. T-stress parameter can also influence the mixed mode I/II fracture process. The T-stress for the ASENB specimen is a function of a/W, S_1/L, and S_2/L and can be expressed as the following equation where T^* is the dimensionless form of T.

$$T = \frac{6PS_1S_2}{tW^2(S_1 + S_2)}T^* \tag{3}$$

The SIFs and T-stress values must be determined for various geometrical and loading conditions in order to characterize the fracture behavior using any specimen. These three parameters are measured in their normalized form (Y_I, Y_{II}, and T^*) by utilizing finite element analyses to analyze the ASENB specimen.

The ABAQUS software was employed to generate the finite element model of the ASENB specimen, which consisted of eight nodded quadratic CPE8 elements. The maximum seed size was set as 1.0 mm and in order to enhance the precision of the numerical results it reduced to 0.05 mm in mid-section. Furthermore, to enhance the precision, singular-type elements with sizes lower than 0.01 mm were employed to model the crack tip region (shown in the red rectangle of Fig. 2). The mesh convergence study shows that the specimens with L/H ratios of 2, 4, 8 and 15, have approximately 30000, 50000, 80,000 and 100,000 elements. Same as actual test conditions, and in accordance with other studies, the supports were simulated using pin and roller supports. Also, the applied load was limited to moving only vertically (same as the fixture of the loading machine) [32–34]. The finite element model of the ASENB sample and a zoomed-in view of the crack tip region are illustrated in Fig. 2.

The geometrical and loading parameters (L/H, a/H, S_1/L, and S_2/L) were considered variables in the numerical analyses. The geometry of ASENB models was selected for the finite element analyses, with length-to-height (L/H) values of 2, 4, 8, and 15, and crack length-to-height (a/H) values of 0.2, 0.4, and 0.6. The S_1/L ratio was set at 0.9 and 0.7, and the S_2/L ratio was adjusted from the symmetric condition ($S_1 = S_2$) to the crack location ($S_1 \gg S_2$). This process was done for each L/H, a/H, *and* S_1/L ratio.

A numerical analysis was conducted by applying a reference load and establishing a contour integral method for crack analysis. The outputs of each scenario were used to extract the corresponding values of stress intensity factors (K_I and K_{II}) and T-stress. The geometrical scenarios that were analyzed are schematically depicted in Fig. 3.

It is important to note that the SIF is frequently achieved at the midpoint of the crack, and the variations for a significant portion of the crack front (excluding the corners) is negligible, as also indicated by other studies [13,24,35].

3. Numerical analysis

The variations of Y_I and Y_{II} values for various L/H, a/H, S_1/L, and S_2/L ratios are depicted in Fig. 4. The pure mode-I fracture condition is indicated by the maximum value of Y_I and zero value of Y_{II} (in the symmetrical condition). The decrement of the S_2/L value results in a decrease in Y_I and an increase in Y_{II} to a specific value of S_2/L, at which point Y_I becomes zero, and Y_{II} reaches the maximum value, indicating the pure mode-II condition.

Looking at the effect of L/H ratios (e.g., 2, 4, 8, and 15), it can be seen with an increase of L/H ratios, the S_2/L ratio for simulating pure mode-I becomes lower significantly. For example, for specimens with $a/H = 0.4$, to simulate the pure mode-II fracture condition, for specimens with L/H

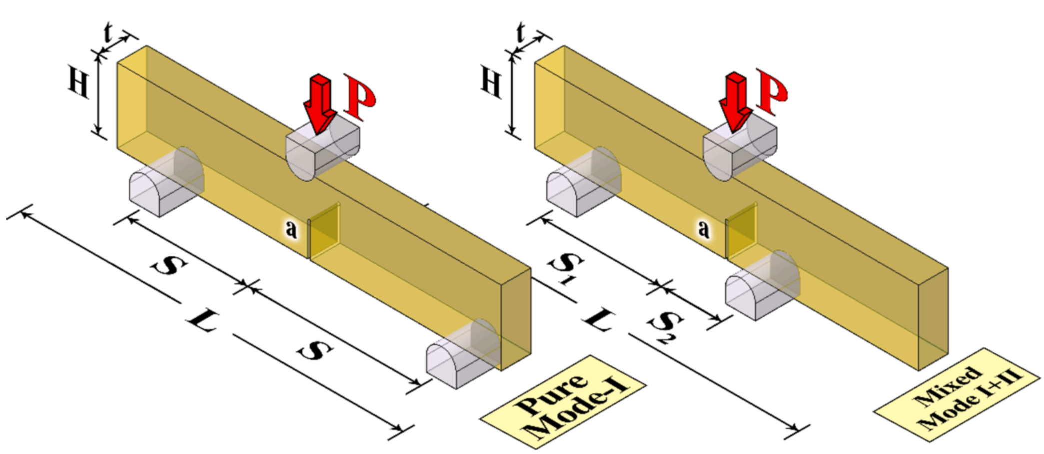

Fig. 1. The form of ASENB specimen and its test configuration for mixed-mode I/II fracture studies.

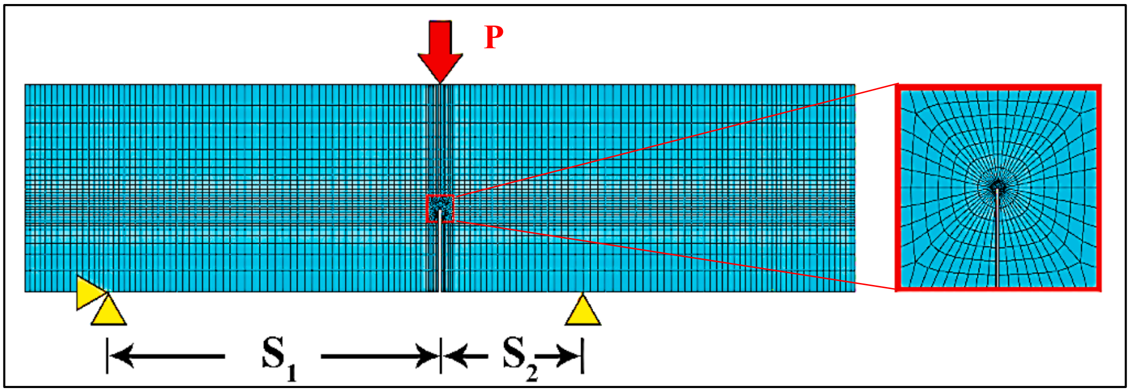

Fig. 2. Finite element model and boundary conditions of ASENB specimen.

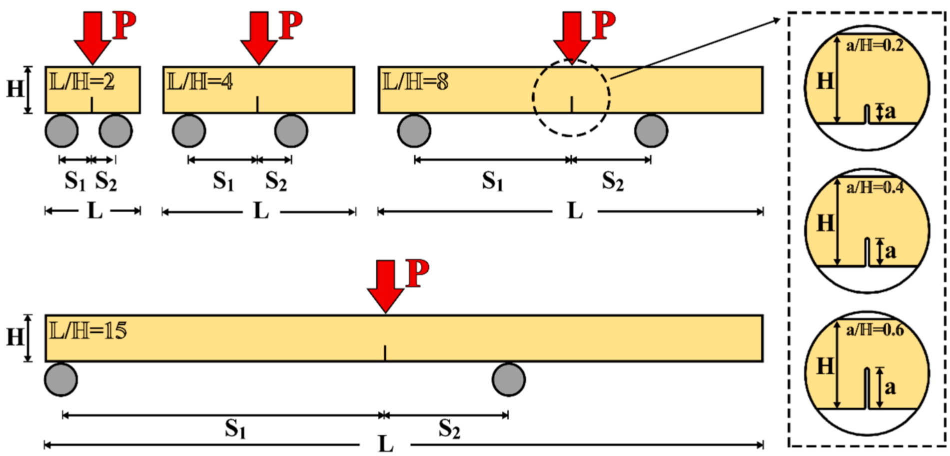

Fig. 3. The assumed geometries for tests of the current study.

$= 2$, the S_2/L ratio should be 0.083, while for specimens with $L/H = 15$, the S_2/L ratio becomes 0.01.

In order to assess the validity of the numerical analysis, the results of the pure mode-I condition were compared with previous studies, and identical results were seen [28–30], also in mixed mode I/II, although the studies are more limited, however, the obtained data is obtained similar to those presented by Aliha et al. [29]. This demonstrates the reliability of the finite element analysis, which encompasses the application of boundary and loading conditions, the mesh pattern, and the extraction of fracture parameters from the current research outputs.

Fig. 5 shows the T^* (non-dimensional T-stress) variations in the ASEND specimen under a variety of geometrical and loading conditions. According to this figure, the corresponding value of T^* increases as the crack length ratio (a/H) or the pure mode II condition is approached. Additionally, the T-stress sign is negative for the ASENB specimen, particularly in dominantly mode II loading conditions, even though there are only a few such cases with slight positive values (dominantly pure mode I loading conditions).

The existence of high negative values of T-stress when approaching the pure mode-II fracture condition suggests that the value of fracture toughness is expected to increase. In this scenario, the effectiveness of the non-singular term (T-stress) in relation to the singular terms (K_I and K_{II}) can be defined by a parameter called the Biaxiality ratio ($B = \frac{T\sqrt{\pi a}}{\sqrt{K_I^2+K_{II}^2}}$).

The variances in the Biaxiality ratio for various geometrical and loading conditions in the analyzed ASENB specimens are shown in Fig. 6. The horizontal axis of these curves is the mode mixity ratio ($M^e = \frac{2}{\pi}tan^{-1}\left(\frac{Y_I}{Y_{II}}\right)$) that shows the dominance of tensile-shear fracture condition by 1 and 0, respectively. As can be seen in Fig. 6, the significant value of the Biaxiality ratio that reaches even -2.5 indicates the substantial impact of T-stress on the mixed mode I/II fracture of materials tested with the ASENB specimen.

It is also worth mentioning, through examination of data, it is seen that expressing the S_2 value relative to the height of the specimen is more direct than the length of the specimen (S_2/H instant of S_2/L). as presented in Fig. 7, which the geometry factors are shown relative to S_2/H value, it is seen, the relative length of specimen (L/H) has the insignificant effect of geometry factors, and geometry factors mostly depend on the relative crack length (a/H). It is also seen that the dependency of geometric factors on relative crack length is more significant for Y_I, and Y_{II} values are even less dependent on relative crack length values.

Examining the fracture parameters (Y_I, Y_{II}, T^*, and B) for the ASENB specimen, considering the S_2 values based on H, it is seen they are nearly insensitive to S_2/H ratio in the range of $0.4 < 2S_2/H$. However, such parameters become much more sensitive with the decrease of S_2/H. This reveals that for producing mode-II fracture conditions (and mode mixities with the dominance of shear mode), the exact placement of support spans (especially S_2) is essential.

As another interesting aspect that is revealed by the use of S_2/H instant of S_2/L values, as can be seen, the relative length of the specimen has an insignificant effect on test configuration. For example, as can be seen, for all the specimens with an a/H ratio of 0.4 (shown as red lines in Fig. 7), the S_2/H value needed to simulate pure mode-II is 0.08. In other words, it is disputed that the specimen has a relative length of $L/H = 2$ or 15; if the specimen's height is constant, the position of S_2 becomes the

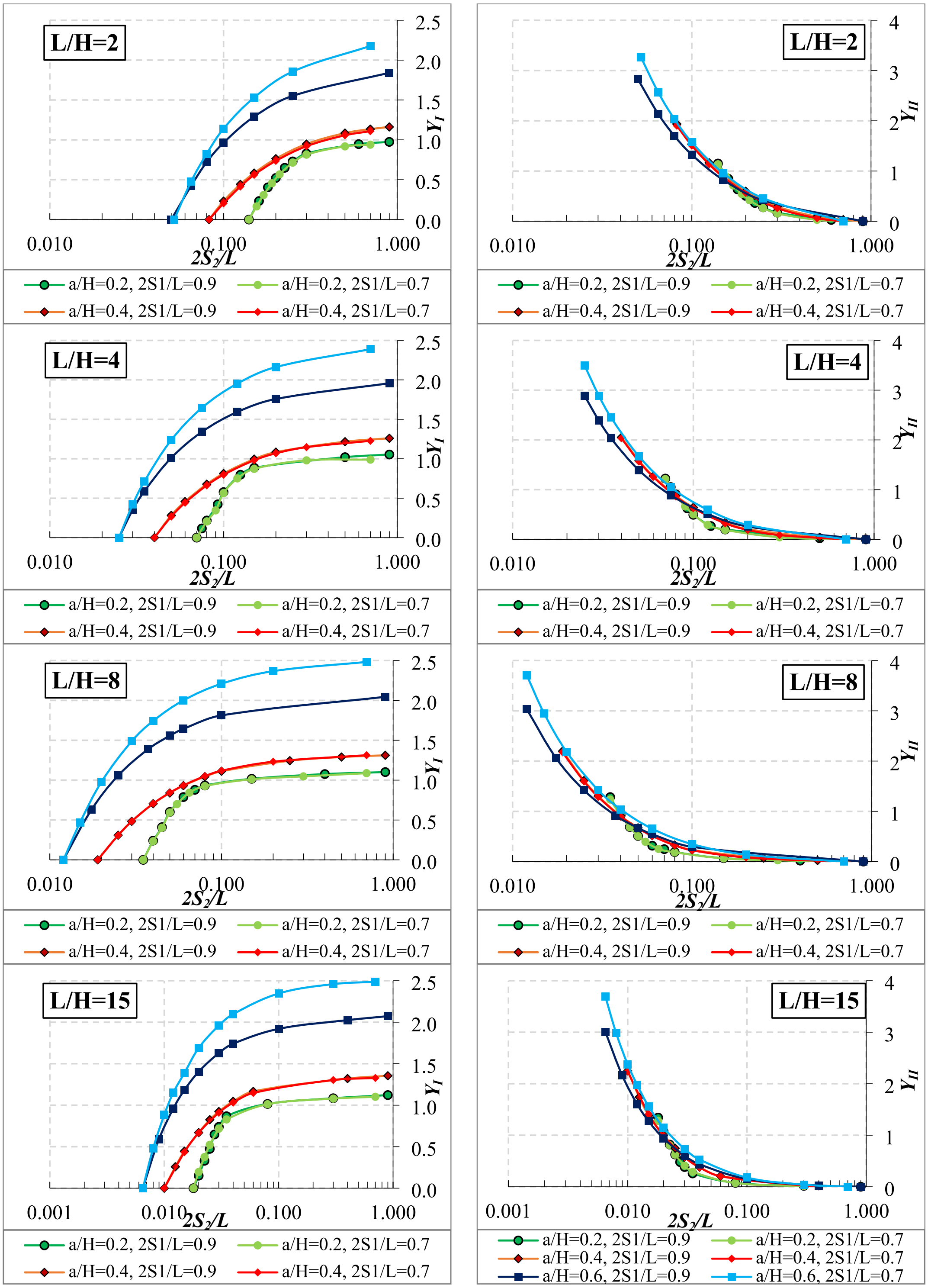

Fig. 4. Variations of Y_I and Y_{II} for the ASENB specimen with different geometries, including crack length ratios (a/H), length ratios (L/H), and loading span ratios (S_1/L and S_2/L).

same. This justifies the use of specimens with lower relative lengths, which also results in the use of lower materials.

4. Experimental fracture tests

In order to investigate the ability of the ASENB specimen, porcelain material in the shape of beams was employed. Porcelain is a ceramic material known for its strength, durability, and homogenously. It is made from a refined clay called kaolin, mixed with other materials like feldspar and quartz. The mixture is fired at high temperatures, typically between 1200 °C and 1400 °C, which vitrifies the material, giving it a glass-like quality and making it non-porous. Porcelain is commonly used for making tiles and decorative objects and is well-known for its fine quality and appeal [36,37].

Porcelain is an excellent material for fracture mechanics tests due to its inherent brittleness, which allows for the study of crack initiation and propagation without plastic deformation. Its homogeneous nature ensures consistent and reproducible fracture behavior, which is crucial for

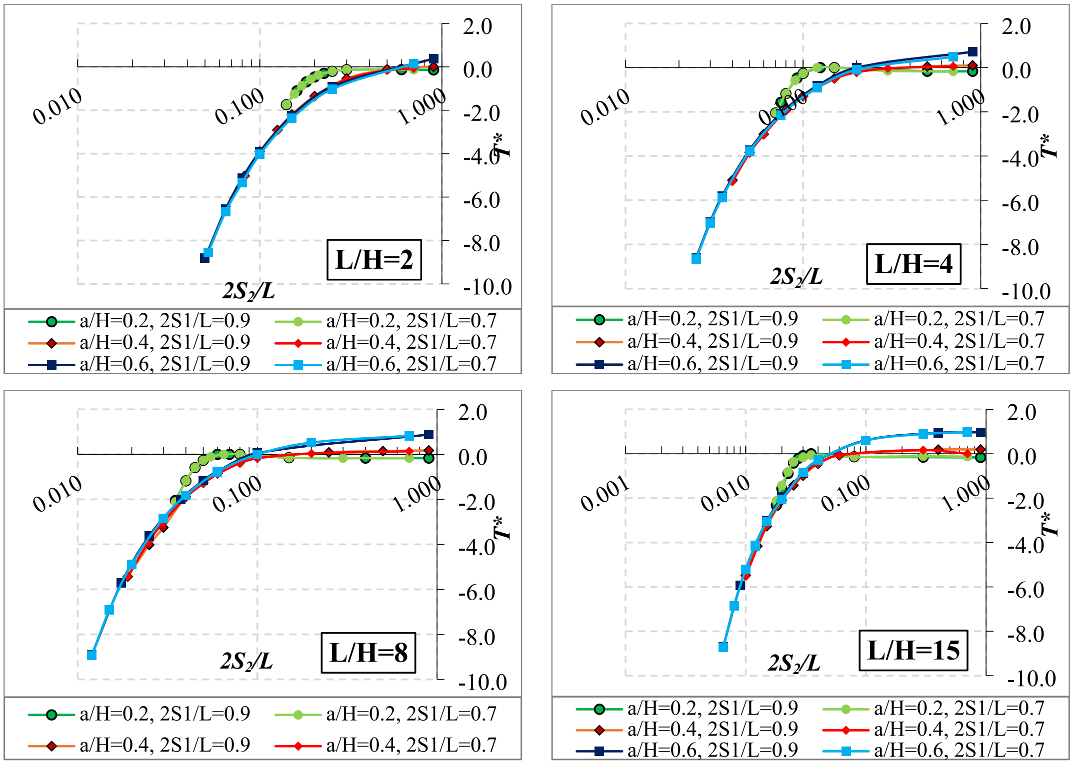

Fig. 5. The values of non-dimensional T-stress (T^*) for the ASENB specimen with different geometries, including crack length ratios (a/W), length ratios (L/H), and loading span ratios (S_1/L and S_2/L).

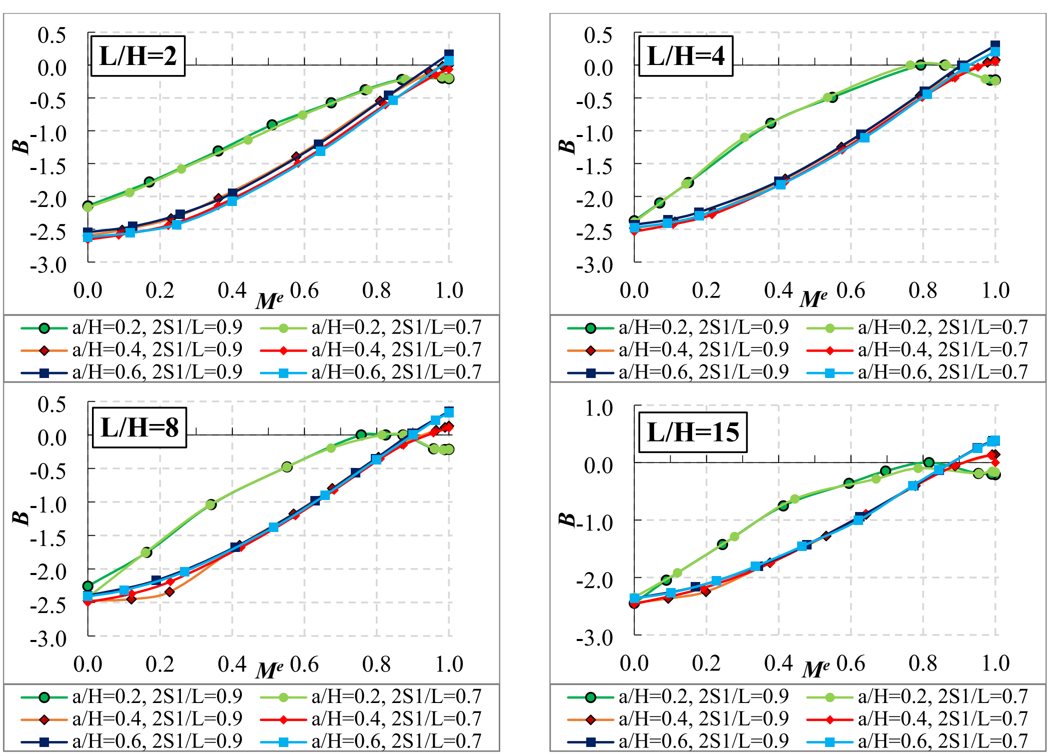

Fig. 6. The changes in Biaxiality ratios relative to mode mixity, for different geometries, including crack length ratios (a/W), length ratios (L/H), and loading span ratios (S_1/L and S_2/L).

reliable test results. Porcelain's well-defined elastic properties facilitate the modeling and analysis of stress and strain behavior under applied loads. Additionally, its fine microstructure is ideal for examining the micro-mechanisms of crack propagation and the influence of microstructural features on fracture behavior. The high strength and hardness of porcelain make it suitable for evaluating fracture toughness under

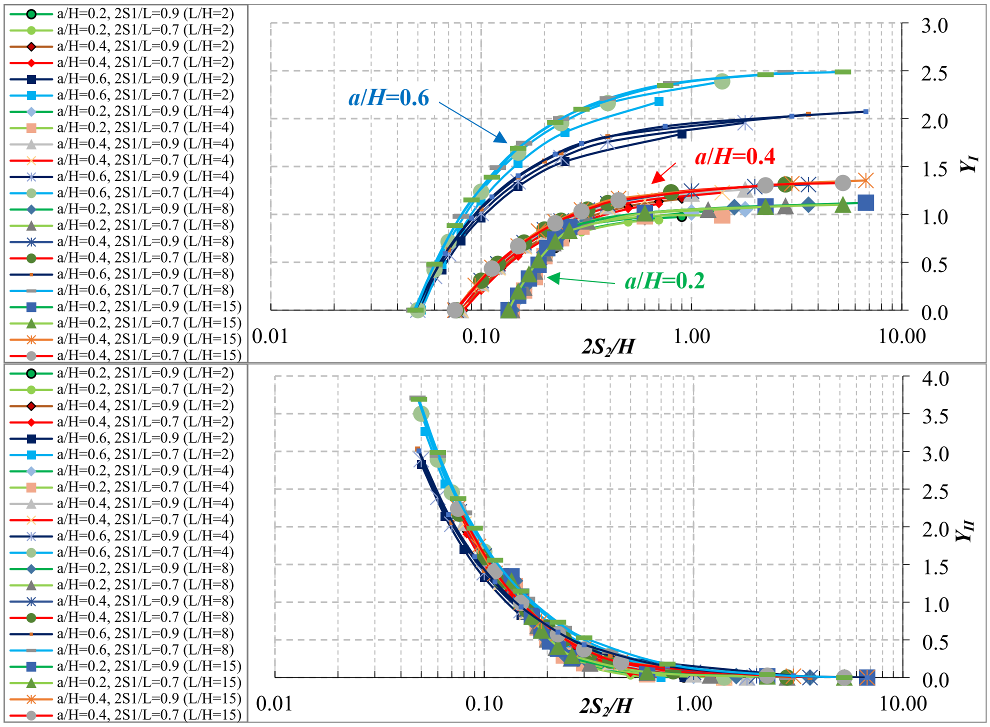

Fig. 7. Variations of geometry factors with S_2/H values in the analyzed ASENB specimen for different geometrical and loading conditions.

various loading conditions. Finally, its availability and ease of processing into test specimens of various shapes and sizes make porcelain a practical choice for experimental investigations into the fracture behavior of brittle materials [38,39].

Initial evaluations and data gathered from the producer show that the used porcelain has a compressive strength of about 770 MPa, a flexural strength of about 95 MPa, and Young's modulus of 55 GPa. It has a 2450 Kg/m3 density and hardness of 6.1 on the Mohs scale. Its Poisson's ratio falls to about 0.23. Chemically, porcelain is composed primarily of 30 % kaolinite ($Al_2Si_2O_5\ (OH)_4$), 25 % of feldspar ($KAlSi_3O_8$), 25 % of quartz (SiO_2) and 20 % of other materials such as clay minerals. It maintains thermal stability at temperatures up to 1200 °C and has a low thermal expansion coefficient of about 3 to 5×10^{-6} /°C. Additionally, its water absorption is minimal, usually less than 0.5 % [40,41].

A sheet of porcelain with a thickness of 10 mm was used to prepare specimens. The height of beam-shaped specimens was chosen as 30 mm, so for simulating the L/H ratios of 2, 4, 8, and 15, beams with lengths of 60, 120, 240, and 450 mm were prepared. As at the middle of the specimen a vertical edge crack is needed, a crack with a length ratio (a/H) of 0.4 was introduced. Same as other studies on brittle materials, these notches were created using a rotary diamond blade with a thickness of 0.2 mm, with the help of a milling machine and adjustable fixture [10,16,24,42].

Mixed-mode fracture experiments were implemented using a three-point bend fixture and test machine, as shown in Fig. 8. There were four distinct M^e values: 1, 0.6, 0.3, and 0.0. the constant loading support (S_1) was set to 0.45L, while the variable loading support (S_2/L) was adjusted for each test condition. A rate of 0.5 mm/min was used to load the specimens. The test was conducted on three replicates for each.

The load–displacement curves of the tested specimens exhibit a linear and brittle behavior under various loading modes, as shown in Fig. 9. It is also evident that the failure load of specimens increases as they transition from pure mode I to pure mode II.

The maximum loads recorded during the tests were placed into Eqs. (1) and (2) to measure the fracture toughness of specimens. Table 1 contains the corresponding geometry factor values (Y_I and Y_{II}) which are necessary for determining the fracture toughness values.

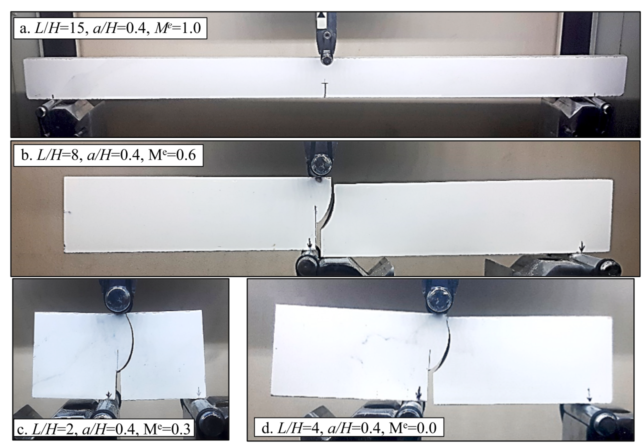

Fig. 8. Test setup for conducting fracture toughness experiments on porcelain material using the ASENB samples, before and after the tests.

The obtained and calculated fracture parameters, including the maximum loads and the fracture toughness values, are shown in Table 2. To assess the validity of the obtained data it is seen, that other studies also measured the fracture toughness of construction porcelain material in the range of 1.0 to 2.0 MPa$\sqrt{m}$ [36,43–45]. it is also interesting, as porcelain is also used vastly in dental applications, the dental porcelain is tested vastly by bio-engineers and due to its higher robustness requirements of dental implants, higher fracture toughnesses are achieved by adding different fillers [46,47].

Fig. 10 shows the variations of fracture toughness for the full range of I/II mode mixities presentation in two absolute and normalized forms. Reviewing the absolute values of fracture toughness for porcelain material shows the value of about 1.4 MPa$\sqrt{m}$, which is in good agreement with other studies that measured it in the range of 1.0 to 2.5 MPa$\sqrt{m}$ [48–50]. The results show that all the specimens (with different L/H values) measured the fracture toughness values almost identical.

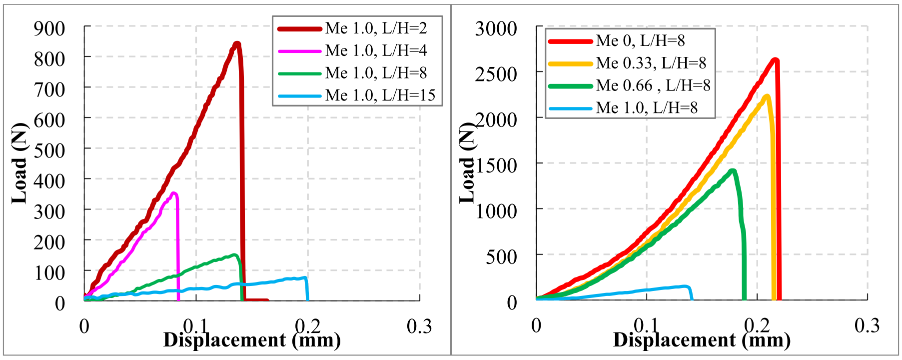

Fig. 9. Examples of load–displacement behaviors seen during the test of porcelain material using ASENB specimen.

Table 1
Geometry factors (Y_I and Y_{II}) for the tested ASENB specimen.

Mode mixity			$M^e = 1.0$	$M^e = 0.6$	$M^e = 0.3$	$M^e = 0.0$
$a/H = 0.4$	$L/H = 2$	$2S_1/L$ (S_1)	0.9 (27 mm)	0.9 (27 mm)	0.9 (27 mm)	0.9 (27 mm)
		$2S_2/L$ (S_2)	0.9 (27 mm)	0.2 (6.0 mm)	0.13 (3.9 mm)	0.0825 (2.5 mm)
		Y_I	0.97	0.75	0.50	0
		Y_{II}	0	0.55	0.98	1.94
		T^*	0.02	−1.35	−2.55	−5.03
$a/H = 0.4$	$L/H = 4$	$2S_1/L$ (S_1)	0.9 (54 mm)	0.9 (54 mm)	0.9 (54 mm)	0.9 (54 mm)
		$2S_2/L$ (S_2)	0.9 (54 mm)	0.1 (6.0 mm)	0.074 (4.0 mm)	0.04 (2.4 mm)
		Y_I	1.23	0.81	0.55	0
		Y_{II}	0	0.60	1.02	2.0
		T^*	0.10	−1.29	−1.6	−5.09
$a/H = 0.4$	$L/H = 8$	$2S_1/L$ (S_1)	0.9 (108 mm)	0.9 (108 mm)	0.9 (108 mm)	0.9 (108 mm)
		$2S_2/L$ (S_2)	0.9 (108 mm)	0.051 (6.1 mm)	0.033 (4.0 mm)	0.02 (2.3 mm)
		Y_I	1.31	0.85	0.58	0
		Y_{II}	0	0.65	1.12	2.17
		T^*	0.17	−1.26	−2.57	−5.43
$a/H = 0.4$	$L/H = 15$	$2S_1/L$ (S_1)	0.9 (202.5 mm)	0.9 (202.5 mm)	0.9 (202.5 mm)	0.9 (202.5 mm)
		$2S_2/L$ (S_2)	0.9 (202.5 mm)	0.027 (6.1 mm)	0.019 (4.0 mm)	0.011 (2.2 mm)
		Y_I	1.33	0.87	0.65	0
		Y_{II}	0	0.66	1.15	2.24
		T^*	0.19	−1.24	−2.68	−5.49

Moving from pure mode-I to mode-II, it is seen that the effective fracture toughness ($K_{eff} = \sqrt{(K_{Ic})^2 + (K_{IIc})^2}$) first decreases (in the range of 1.0 $< M^e <$ 0.3) and then increases significantly. So that, for M^e values of 1.0, 0.6, 0.3, and 0.0, the values of K_{eff} calculate averagely as 1.37, 1.25, 1.40, and 1.72.

Fig. 10(b) shows the normalized form of fracture toughness values. This figure demonstrates that moving from pure mode-I to pure mode-II, the fracture toughness value increases such that the K_{IIc} value reaches 1.25 times the K_{Ic}. In order to evaluate the validity of the trend, in Fig. 10, the predictions of two mixed mode fracture theories are also shown. However, the difference between these two well-known criteria should be evaluated first.

Considering the formula for calculating the tangential stress component ($\sigma_{\theta\theta}$) at the crack tip (with r, θ coordinates) as the following equation (known as a Williams series), the MTS criteria only considers the first term of the equation and neglects the term that participates the T-stress (non-singular term) effect. This is while, in GMTS criteria, both the singular and non-singular terms are considered.

$$\sigma_{\theta\theta} = \frac{1}{\sqrt{2\pi r}} cos\frac{\theta}{2}\left[K_I cos^2\frac{\theta}{2} - \frac{3}{2}K_{II} sin\theta\right] + Tsin^2\theta + higher\ order\ terms \quad (4)$$

As can be observed in Fig. 10, the maximum tangential stress (MTS) criterion can't provide suit predictions, and the discrepancy between the test results and theoretical estimations risers moving toward pure mode II, while general maximum tangential stress (GMTS) accurately predicts trends in all the trend of mixed mode I/II. Indeed, as described before, the effect of T-stress (that is ignored in the MTS criterion) is the reason for the discrepancy between the predictions of the theories [51].

Solving the EQ.4 for the critical value of fracture load and defining r_c as the critical distance from the crack tip, when the tangential stress at the crack's tip reaches a critical value ($\sigma_{\theta\theta c}$), the general equation of the

Table 2
Maximum loads and K_{Ic}, K_{IIc}, K_{eff} and T_c values.

a/H	L/H	M^e	$P_{c\ avg}$ (N)	COV	$K_{Ic,avg}$ (MPa$\sqrt{m}$)	$K_{IIc,avg}$ (MPa$\sqrt{m}$)	K_{eff} (MPa$\sqrt{m}$)	$T_{c\ avg}$ (MPa)
$a/H = 0.4$	$L/H = 2$	1.0	825	14 %	1.35	0.00	1.35	0.12
		0.6	2102	7 %	0.96	0.71	1.20	−7.74
		0.3	2924	8 %	0.62	1.22	1.37	−14.12
		0.0	3256	13 %	0.00	1.78	1.78	−20.63
$a/H = 0.4$	$L/H = 4$	1.0	332	9 %	1.37	0.00	1.37	0.50
		0.6	1925	8 %	1.05	0.78	1.31	−7.45
		0.3	2357	11 %	0.66	1.23	1.40	−13.97
		0.0	3035	10 %	0.00	1.74	1.74	−19.72
$a/H = 0.4$	$L/H = 8$	1.0	154	10 %	1.36	0.00	1.36	0.79
		0.6	1616	9 %	0.99	0.76	1.25	−6.55
		0.3	2367	13 %	0.65	1.26	1.42	−12.91
		0.0	2758	13 %	0.00	1.66	1.66	−18.58
$a/H = 0.4$	$L/H = 15$	1.0	83	11 %	1.39	0.00	1.39	0.89
		0.6	1558	6 %	1.00	0.76	1.25	−6.33
		0.3	2047	15 %	0.69	1.23	1.41	−12.76
		0.0	2746	6 %	0.00	1.70	1.70	−18.64

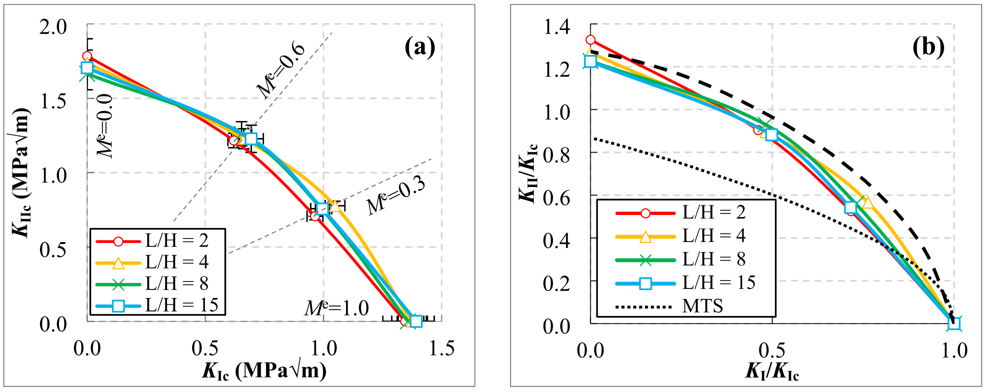

Fig. 10. A) the absolute values of fracture toughness values obtained by the test of asenb specimens made of porcelain material. b) the normalized form of fracture toughness values, along with prediction curves of mts and gmts criteria.

GMTS criterion can be written as:

$$\frac{\partial\sigma_{\theta\theta}}{\partial\theta}=0,\ \frac{\partial^2\sigma_{\theta\theta}}{\partial\theta^2}<0\quad\left[K_I sin\frac{\theta}{2}-K_{II}(3cos\theta-1)\right]-\frac{16T}{3}\sqrt{2\pi r_c}cos\theta sin\frac{\theta}{2}=0 \tag{5}$$

$$K_{Ic}=cos\frac{\theta}{2}\left[K_I cos^2\frac{\theta}{2}-\frac{3}{2}K_{II}sin\theta\right]+\sqrt{2\pi r_c}Tsin^2\theta \tag{6}$$

As seen in these equations, besides the magnitude of *T*-stress in the GMTS criterion, it also has a role. So that the fracture toughness value increases for negative *T*-stress values and decreases for its positive values. This statement was also concluded by other researchers utilizing other specimens with negative and positive *T*-stress.

Similarly, the direction of crack initiation decreases with negative *T*-stress and vice versa. The direction of crack initiation (θ) for the tested material can be predicted by utilizing fracture parameters (i.e., K_I, K_{II}, and T). Fig. 11 shows fractured ASENB samples with varying mode mixities. The fracture is observed to deviate from its vertical direction and propagate along a curvilinear trajectory, with the exception of pure mode I. As mixed mode progresses toward pure mode II, the angle of fracture initiation increases.

Fig. 12 presents the direction of crack initiation recorded after the test, along with its theoretical values calculated using the MTS and GMTS criteria. It is seen that the GMTS criterion presents acceptable estimations for the directions of crack initiation in all tested mode mixities compared to the MTS. Measured from the test samples, similar to predictions of GMTS criteria, the crack initiation direction for M^e values of 1, 0.6, 0.3, and 0 ratios was obtained as 0, −52, −70, and −82 degrees. This is while MTS criteria predict the crack initiation angles about 10 % lower than its actual value. Similar to fracture toughness values, this prediction difference arises due to significant negative T-stress.

To assess the trends seen for experimental data of current research, looking at other studies is helpful. In this regard, the trend of data and its

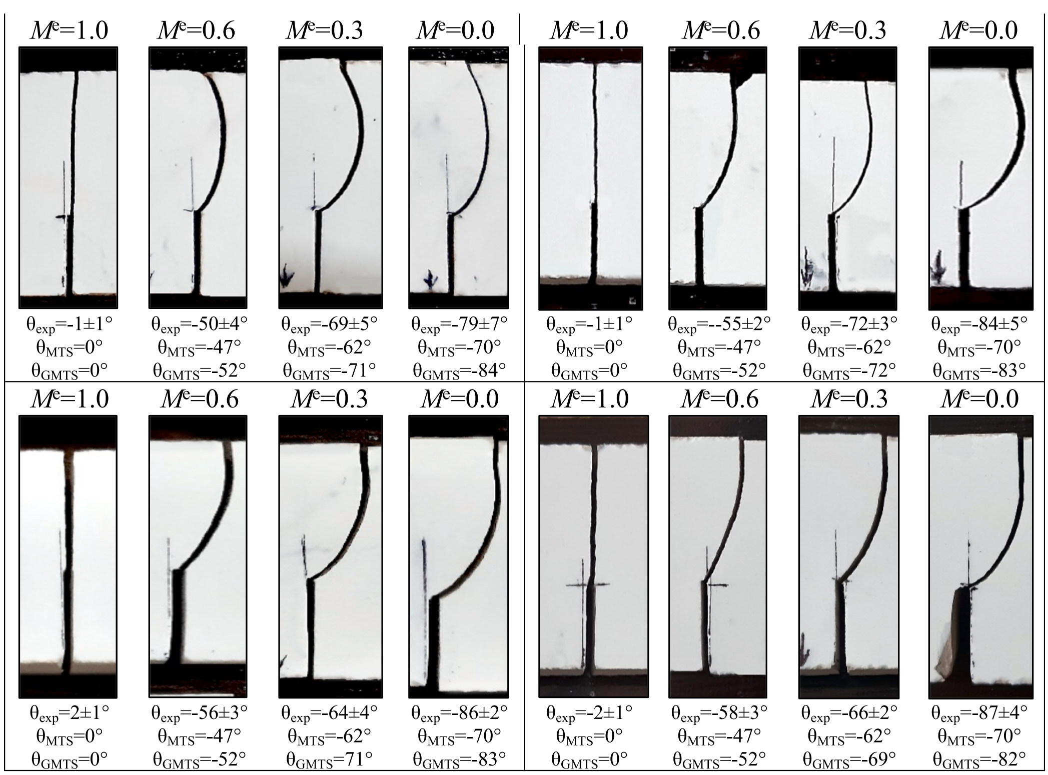

Fig. 11. Crack initiation direction of tested ASENB samples, along with MTS and GMTS predictions for the crack initiation angles.

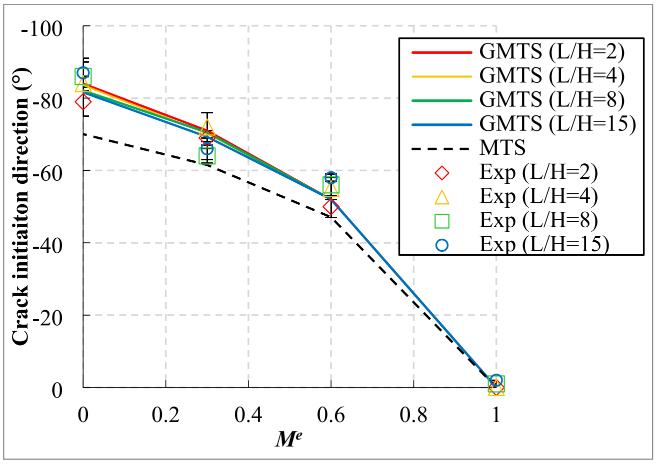

Fig. 12. Comparison of crack initiation angles for mixed mode fracture behavior, along with predictions of GMTS and MTS criteria.

prediction with fracture criteria, including the ratio of fracture toughness in pure mode-I to pure mode-II or crack initiation angle was in accordance with previous studies [52–55]. It is worth mentioning, that researchers have also seen the same trends using other specimens such as Brazilian disc or semi-circular bend specimens [55–58].

As a summary of the experiment section, SENB is a suitable specimen for fracture tests of many materials, especially those that can be extracted from sheets. Preparation of SENB is straightforward, and its test does not need complex fixtures. More especially, all the I-II mixed-mode (including pure mode-I and II) can simulated by only adjusting the supports.

To suggest an optimal geometry for the SENB specimen, as the results showed, the relative length (length to height ratio) of the SENB specimens hasn't a significant effect on the fracture results in all the mixed mode I-II conditions. In this condition in line with studies such as Mousavi et al. [27] and Aliha et al. [28], in the dominant mode-I condition, and for the sake of minimizing the needed material for preparing the samples, using compact specimens with $L/H \leq 2$ is practical. this is, however, dictating the asymmetrical loading condition and closeness of one support to the crack plane in dominant mod-II fracture, a minimum $L/H = 4$ ratio is more practical for the tests.

5. Conclusions

The Single-edge Notched Beam (SENB) is a widely used specimen for measuring fracture-related parameters in brittle materials. However, due to the absence of a well-known testing configuration, researchers have employed SENB with various geometries, particularly differing in the length-to-height (L/H) ratios. This research evaluated the effect of SENB's geometry on mode I/II fracture parameters numerically and experimentally. From the results, the following conclusions can be drawn.

- The corresponding value of T^* increases with the increase of crack length ratio (a/H) and by moving toward pure mode II condition.
- The T-stress sign is negative for the ASENB specimen, particularly in dominantly mode II loading condition, which show that the fracture toughness value is expected to increase. However, a few cases with slight positive values (dominantly pure mode I loading conditions) are seen.
- With increased L/H ratios, the S_2/L ratio for simulating pure mode-I becomes significantly lower. However, expressing the S_2 value relative to the height of the specimen is more direct than the length of the specimen (S_2/H instant of S_2/L).
- Considering the S_2/H ratio for determining test configuration, fracture parameters were insensitive to the S_2/H ratio for $0.4 < 2S_2/H$. However, they become intensely more sensitive with decreased S_2/H.
- The relative length of the specimen has an insignificant effect on test configuration. For all the specimens with a constant a/H ratio, the S_2/H value becomes constant, which justifies using specimens with lower relative lengths.
- The porcelain's mode-I fracture toughness (K_{Ic}) values were about 1.4 MPa$\sqrt{\text{m}}$. All specimens almost identically measured the fracture toughness values.
- Moving from pure mode-II, the effective fracture toughness first decreases (in the $1.0 < M^e < 0.3$) and then increases significantly. For M^e values of 1.0, 0.6, 0.3, and 0.0, K_{eff}'s values are 1.37, 1.25, 1.40, and 1.72 MPa$\sqrt{\text{m}}$.
- The maximum tangential stress (MTS) criterion couldn't provide suitable predictions of data trends. General maximum tangential stress (GMTS) accurately predicts trends. The effect of T-stress (ignored in the MTS criterion) is the reason for the discrepancy between the predictions of these theories.
- When moving toward pure mode-II condition, the fracture is observed to deviate from its vertical direction and propagate along a curvilinear trajectory. As mixed mode progresses toward pure mode II, the angle of fracture initiation increases.
- As predicted by theoretical criteria, as observed in experimental tests, in pure mode II, the crack initiation angle reaches up to 80° (relative to the pre-crack axis), indicating a significant effect of negative T-stress.

CRediT authorship contribution statement

Tang Qiong: Conceptualization, Investigation, Methodology, Supervision, Writing – original draft. **Haytham F. Isleem:** Writing – original draft, Methodology, Investigation, Formal analysis, Software, Visualization. **Hamid Reza Karimi:** Writing – review & editing, Supervision, Project administration, Methodology, Formal analysis, Conceptualization.

Declaration of competing interest

The authors declare that they have no known competing financial interests or personal relationships that could have appeared to influence the work reported in this paper.

Data availability

Data will be made available on request.

References

[1] J. Zhou, A. Pellegrino, V.L. Tagarielli, A new technique to measure the dynamic fracture toughness of solids, Polym. Test 127 (2023) 108198, https://doi.org/10.1016/j.polymertesting.2023.108198.
[2] X. Zhou, X. Liu, X. Wang, Z. Gu, H. Xie, S. Zhang, Mechanical and fracture characteristics in center cracked circular discs of coal specimens with different sizes: An experimental investigation, Theor. Appl. Fract. Mech. 129 (2024) 104245, https://doi.org/10.1016/j.tafmec.2023.104245.
[3] M.R.M. Aliha, H.G. Kouchaki, M.H. Mohammadi, P.J. Haghighatpour, N. Choupani, P. Asadi, M. Akbari, M.G. Darvish, T. Sadowski, Fracture toughness determination for epoxy-based polymer concrete mixtures: Applicability of different rectangular beam and circular disc specimens, Composites Part c: Open Access 14 (2024) 100446, https://doi.org/10.1016/j.jcomc.2024.100446.
[4] S.G. Hosseini, A. Abdi Kordani, M. Zarei, Effect of recycled additives on pure mode I fracture resistance and moisture susceptibility of hot mix asphalt (HMA): An experimental study using semicircular bending (SCB), in: And Indirect Tensile Strength (ITS) Tests, Theoretical and Applied Fracture Mechanics 128, 2023, p. 104168, https://doi.org/10.1016/j.tafmec.2023.104168.
[5] X. Han, Q. Xiao, K. Cui, X. Hu, Z. Zhou, Determining the fracture toughness of quasi-brittle materials with notched four-point bending tests, Eng Fract Mech 284 (2023) 109259, https://doi.org/10.1016/j.engfracmech.2023.109259.

[6] J. Zheng, H. Li, J.D. Hogan, Advanced tensile fracture analysis of alumina ceramics: Integrating hybrid finite-discrete element modeling with experimental insights, Eng. Fract. Mech. 302 (2024) 110075, https://doi.org/10.1016/j.engfracmech.2024.110075.

[7] D. Ma, Y. Wu, X. Ma, X. Hu, W. Dong, D. Li, L. Li, Fracture behavior of sandstone with partial filling flaw under mixed-mode loading: Three-point bending tests and discrete element method (DEM) numerical approach, J. Rock Mech. Geotech. Eng. (2024), https://doi.org/10.1016/j.jrmge.2023.12.034.

[8] A. Coq, J. Diani, Comparison of Mode I fracture toughness of an elastic and an elastoplastic methyl methacrylate polymer as measured by SENB and DCDC tests, Eng Fract Mech 306 (2024) 110237, https://doi.org/10.1016/j.engfracmech.2024.110237.

[9] Q. Lin, X. Bian, P.-Z. Pan, Y. Gao, Y. Lu, Criterion of local symmetry visualized in small eccentric single edge notched bend (E-SENB) rock specimens, Eng. Fract. Mech. 248 (2021) 107709, https://doi.org/10.1016/j.engfracmech.2021.107709.

[10] H.R. Karimi, E. Khedri, A. Mousavi, A. Taherifar, Z. Abdoli, R. Mohamadi, Mode I/II cracking behavior of additively manufactured interpenetrating phase composites (IPC), an experimental and theoretical study, Theor. Appl. Fract. Mech. 131 (2024) 104396, https://doi.org/10.1016/j.tafmec.2024.104396.

[11] A. Zeinedini, M.M. Shokrieh, A. Ebrahimi, The effect of agglomeration on the fracture toughness of CNTs-reinforced nanocomposites, Theor. Appl. Fract. Mech. 94 (2018) 84–94, https://doi.org/10.1016/j.tafmec.2018.01.009.

[12] H. Taghibeigi, A. Zeinedini, A.H. Oleiwi, On the mixed mode I/II translaminar fracture of plain-weave carbon, E-glass and Kevlar reinforced laminated composites, Compos Sci Technol 241 (2023) 110117, https://doi.org/10.1016/j.compscitech.2023.110117.

[13] H. Haeri, V. Sarfarazi, P. Ebneabbasi, M.R.M. Aliha, G. Saeedi, H.R. Karimi, A. M. Far, Edge notched disc test for evaluation of mode-I fracture toughness of brittle material, J. Mater. Res. Technol. (2023), https://doi.org/10.1016/j.jmrt.2023.10.322.

[14] S. Ghafari, F.M. Nejad, A. Sheikh-Akbari, H. Kazemi, Automating the determination of low-temperature fracture resistance curves of normal and rubberized asphalt concrete in single-edge notched beam tests using convolutional neural networks, Constr. Build Mater. 428 (2024) 136376, https://doi.org/10.1016/j.conbuildmat.2024.136376.

[15] H.-C. Dan, Z. Zhang, J. Chen, W. Cao, Low-temperature fracture characteristics of asphalt mixtures using the eccentric single-edge notched bend test: A 3D discrete element study, Constr. Build Mater. 344 (2022) 128182, https://doi.org/10.1016/j.conbuildmat.2022.128182.

[16] E. Khedri, H. reza Karimi, M.R.M. Aliha, N. Nazemzadeh, B. Talebi, R. Aleali, Tensile, flexural, and mode-I cracking behavior of interpenetrating phase composites (IPC), developed using additively manufactured PLA-based structures with different infill densities and epoxy resin polymer as matrix, Results Eng. 22 (2024) 102162, https://doi.org/10.1016/j.rineng.2024.102162.

[17] N. Shabakhty, H.R. Karimi, A. Yeganeh-Bakhtiary, Statistical evaluation of fracture and mechanical performance of engineered cementitious composites (ECC), containing different percentages of glass, polypropylene, polyvinyl-alcohol fibers, and fly ash, Constr. Build Mater. 417 (2024) 135247.

[18] M.R.M. Aliha, H.R. Karimi, M. Abedi, The role of mix design and short glass fiber content on mode-I cracking characteristics of polymer concrete, Constr. Build Mater. 316 (2022) 125590.

[19] N. Shabakhty, H.R. Karimi, A.Y. Bakhtiary, Cementitious composites in aquatic environments, evaluation of fracture and mechanical behavior in long-term submerging in fresh and saltwater, and simulated splash zone conditions, Case Stud. Constr. Mater. (2024) e03035.

[20] A.K. Mishra, A. Lambai, V. Jayaram, B.N. Jaya, The edge-notched clamped beam bend specimen as a fracture toughness test geometry, Theor. Appl. Fract. Mech. 105 (2020) 102409, https://doi.org/10.1016/j.tafmec.2019.102409.

[21] X. Wang, A. Atkinson, On the measurement of ceramic fracture toughness using single edge notched beams, J. Eur. Ceram. Soc.. 35 (2015) 3713–3720, https://doi.org/10.1016/j.jeurceramsoc.2015.05.005.

[22] E. Khedri, H.R. Karimi, R. Mohamadi, M.R.M. Aliha, R. Masoudi Nejad, Mechanical, fracture, and environmental performance of greener polymer composites containing low to high micro fillers with recycled and byproduct origins, Polym. Compos. n/a (2024). DOI: 10.1002/pc.28369.

[23] H. Aalinejadian, M.R.M. Aliha, M. Ameri, H.R. Karimi, P. Jafari Haghighatpour, N. Choupani, Comparison of mixed mode I/III fracture toughness data obtained from the ENDB specimens manufactured by gyratory cylinders with two diameters of 100 and 150 mm, Int. J. Pavement Eng. 24 (2023) 2281996, https://doi.org/10.1080/10298436.2023.2281996.

[24] E. Karimi, M.R.M. Khedri, A. Aliha, Mousavi, A comprehensive study on ring shape specimens under compressive and tensile loadings for covering the full range of I+II fracture modes of gypsum material, Int. J. Rock Mech. Min. Sci. 160 (2022) 105265, https://doi.org/10.1016/j.ijrmms.2022.105265.

[25] J. Karimi, M.R.M. Bidadi, A. Aliha, M.H. Mousavi, P. Mohammadi, Jafari Haghighatpour, An experimental study and theoretical evaluation on the effect of specimen geometry and loading configuration on recorded fracture toughness of brittle construction materials, J. Build. Eng. 75 (2023) 106759, https://doi.org/10.1016/j.jobe.2023.106759.

[26] M.R.M. Aliha, S.S. Mousavi, Sub-sized short bend beam configuration for the study of mixed-mode fracture, Eng. Fract. Mech. 225 (2020) 106830.

[27] S.S. Mousavi, M.R.M. Aliha, D.M. Imani, On the use of edge cracked short bend beam specimen for PMMA fracture toughness testing under mixed-mode I/II, Polym. Test 81 (2020) 106199.

[28] M.R.M. Aliha, S.S. Samareh-Mousavi, M.M. Mirsayar, Loading rate effect on mixed mode I/II brittle fracture behavior of PMMA using inclined cracked SBB specimen, Int. J. Solids Struct. 232 (2021) 111177, https://doi.org/10.1016/j.ijsolstr.2021.111177.

[29] M.R.M. Aliha, H.R. Karimi, S.M.N. Ghoreishi, Design and validation of simple bend beam specimen for covering the full range of I+II fracture modes, Eur. J. Mech. A. Solids 104425 (2021).

[30] S.A. Saed, H.R. Karimi, S. Mousavirad, M.R.M. Aliha, X. Shi, P.J. Haghighatpour, Full range I/II fracture behavior of asphalt mixtures containing RAP and rejuvenating agent using two different 3-point bend type configurations, Constr. Build Mater. 314 (2022) 125590.

[31] M. Aghababaei, M. Behnia, M.R.M. Aliha, Experimental investigation on the effect of grain size of granitic rocks on the fracture roughness and toughness, Geomech. Energy Environ. 38 (2024) 100535, https://doi.org/10.1016/j.gete.2024.100535.

[32] M. Bakhshizadeh, S. Pirmohammad, H.R. Karimi, M.R.M. Aliha, Effect of support friction on pure mode I, II, and III fracture toughness of cement concrete tested with edge-notched disc bend specimen, Theor. Appl. Fract. Mech. 129 (2024) 104247, https://doi.org/10.1016/j.tafmec.2023.104247.

[33] L. Tutluoglu, C. Karatas Batan, M.R.M. Aliha, Tensile mode fracture toughness experiments on andesite rock using disc and semi-disc bend geometries with varying loading spans, Theor. Appl. Fract. Mech. 119 (2022) 103325, https://doi.org/10.1016/j.tafmec.2022.103325.

[34] H. Wang, H. Li, L. Tang, C. Zhu, X. Ren, Y. Qiao, G. Feng, Fracture of brittle solid with an internal penny-shaped crack: Semi-circular bending test and numerical simulation, Eng. Fract. Mech. 262 (2022) 108260, https://doi.org/10.1016/j.engfracmech.2022.108260.

[35] J. Fu, H. Haeri, J.F. Labuz, V. Sarfarazi, P. Ebneabbasi, M.R.M. Aliha, H.R. Karimi, S. Jahanmiri, M.F. Marji, Determination of mode I fracture toughness of brittle materials with a new method, Acta Mech. Sinica 40 (2023) 423236, https://doi.org/10.1007/s10409-023-23236-x.

[36] X. Xu, A. Li, J. Wu, Y. Yin, S. Ma, J. Yuan, Effect of zirconia addition amount in glaze on mechanical properties of porcelain slabs, Ceram. Int. 49 (2023) 20080–20087, https://doi.org/10.1016/j.ceramint.2023.03.131.

[37] J. Atidi, H. Kasedde, E. Menya, P.W. Olupot, Optimization of physical and mechanical properties of porcelain tiles from coffee parchment husk ash, J. Eng. Res. (2023), https://doi.org/10.1016/j.jer.2023.11.013.

[38] K. Kim, B. Moon, D. Kim, K. Park, C.-S. Seok, T. Kim, J. Yi, I.-H. Choi, Mechanical property evaluation according to alumina content of aged porcelain insulator, J. Mater. Res. Technol. 9 (2020) 9777–9783, https://doi.org/10.1016/j.jmrt.2020.06.075.

[39] B. Nascimento de Souza, M. Dal Bó, D. Hotza, M.C. Fredel, Chemical modification of porcelain tile surface to optimize flexural strength and Weibull modulus through the ion exchange process, J. Build. Eng. 56 (2022) 104735, https://doi.org/10.1016/j.jobe.2022.104735.

[40] X. Zhong, L. Cao, J. Huang, Y. Liu, X. Shen, Q. Wang, Formula optimization and mechanical properties of thin porcelain ceramic plates mainly containing smoky quartz tailings, Ceram. Int. 48 (2022) 24056–24062, https://doi.org/10.1016/j.ceramint.2022.05.085.

[41] N.S. Mehta, S. Dey, V. Singh, M.R. Majhi, Analysis the effect of TiO2 addition on sintering, physical mechanical behavior of porcelain insulating material, Appl. Surf. Sci. Adv. 4 (2021) 100083, https://doi.org/10.1016/j.apsadv.2021.100083.

[42] M.R. Hadei, N. Akbarlou, H.R. Nejati, A new development cracked chevron notched direct tension method for determining the mode I fracture toughness of rocks, Theor. Appl. Fract. Mech. 110 (2020) 102811, https://doi.org/10.1016/j.tafmec.2020.102811.

[43] M.R. Ayatollahi, M.R.M. Aliha, Fracture Analysis of Some Ceramics Under Mixed Mode Loading, J. Am. Ceram. Soc. 94 (2011) 561–569, https://doi.org/10.1111/j.1551-2916.2010.04076.x.

[44] A.R. Rosenfield, Fracture of Brittle Materials under a Simulated Wear Stress System, J. Am. Ceram. Soc. 72 (1989) 2117–2120, https://doi.org/10.1111/j.1151-2916.1989.tb06041.x.

[45] A. Schellenberger, R. Belli, J. Karsten, U. Lohbauer, On the robustness of the Single-Edge-Precracked-Beam (SEPB) method for fracture toughness testing of ceramic materials, Eng. Fract. Mech. 291 (2023) 109527, https://doi.org/10.1016/j.engfracmech.2023.109527.

[46] T. Sato, K. Tsuji, N. Kawashima, H. Sato, Y. Nakamura, Effect of defect size on fracture strength of dental low fusion porcelain, Colloids Surf. B Biointerf. 38 (2004) 77–82, https://doi.org/10.1016/j.colsurfb.2004.07.015.

[47] S.N. White, C.C. Green, R.M. McMeeking, A simple 3-point flexural method for measuring fracture toughness of the dental porcelain to zirconia bond and other brittle bimaterial interfaces, J. Prosthodont. Res. 64 (2020) 391–396, https://doi.org/10.1016/j.jpor.2019.11.002.

[48] G.A. Gogotsi, Fracture toughness of ceramics and ceramic composites, Ceram. Int. 29 (2003) 777–784, https://doi.org/10.1016/S0272-8842(02)00230-4.

[49] S.R. Bragança, C.P. Bergmann, H. Hübner, Effect of quartz particle size on the strength of triaxial porcelain, J. Eur. Ceram. Soc. 26 (2006) 3761–3768, https://doi.org/10.1016/j.jeurceramsoc.2006.01.012.

[50] H. Wang, P. Pallav, G. Isgrò, A.J. Feilzer, Fracture toughness comparison of three test methods with four dental porcelains, Dent. Mater. 23 (2007) 905–910, https://doi.org/10.1016/j.dental.2006.06.033.

[51] A. Zeinedini, A novel fixture for mixed mode I/II/III fracture testing of brittle materials, Fatigue Fract. Eng. Mater. Struct. 42 (2019) 838–853, https://doi.org/10.1111/ffe.12955.

[52] W. Hua, J. Li, Z. Zhu, A. Li, J. Huang, Z. Gan, S. Dong, A review of mixed mode I-II fracture criteria and their applications in brittle or quasi-brittle fracture analysis, Theor. Appl. Fract. Mech. 124 (2023) 103741, https://doi.org/10.1016/j.tafmec.2022.103741.

[53] E. Bura, A.R. Torabi, A. Seweryn, Fracture prediction in flat PMMA notched specimens under tension - effectiveness of the equivalent material concept and fictitious material concept, Theor. Appl. Fract. Mech. 130 (2024) 104273, https://doi.org/10.1016/j.tafmec.2024.104273.
[54] Y. Wu, T. Yin, D. Zhuang, Y. Chen, J. Ma, W. Guo, Initial and unstable fracture toughness of quartz-diorite rock under mixed mode I/II loading: Experimental and numerical investigation, Theor. Appl. Fract. Mech. 127 (2023) 104079, https://doi.org/10.1016/j.tafmec.2023.104079.
[55] Z. Zhan, Y. Yu, W. Yao, K. Xia, Validity for measuring mode II fracture toughness using the short beam in compression method, Eng. Fract. Mech. 308 (2024) 110381, https://doi.org/10.1016/j.engfracmech.2024.110381.
[56] P. Cao, T. Zhou, Y. Ju, J. Zhu, Mixed mode I/II fracture behavior of CSTBD sandstone specimen under different loading angles, Geomech. Geophys. Geo-Energy Geo-Res. 9 (2023) 54, https://doi.org/10.1007/s40948-023-00590-8.
[57] M. Marghitas, L. Marsavina, C.-F. Popa, R. Brighenti, On the mixed mode fracture of DLP manufactured SCB specimens, Proc. Struct. Integrity 56 (2024) 26–32, https://doi.org/10.1016/j.prostr.2024.02.033.
[58] S. Pirmohammad, R. Momeni, S.H. Khanghahi, Effect of SCB specimen size on mode I fracture parameters of asphalt concrete at low and intermediate temperatures, Theor. Appl. Fract. Mech. 130 (2024) 104314, https://doi.org/10.1016/j.tafmec.2024.104314.